Numerical Bifurcation Analysis of Homoclinic Orbits Embedded in One-Dimensional Manifolds of Maps

NIELS NEIRYNCK and WILLY GOVAERTS, Ghent University
YURI A. KUZNETSOV, Utrecht University and University of Twente
HIL G. E. MEIJER, University of Twente

We describe new methods for initializing the computation of homoclinic orbits for maps in a state space with arbitrary dimension and for detecting their bifurcations. The initialization methods build on known and improved methods for computing one-dimensional stable and unstable manifolds. The methods are implemented in MatContM, a freely available toolbox in Matlab for numerical analysis of bifurcations of fixed points, periodic orbits, and connecting orbits of smooth nonlinear maps. The bifurcation analysis of homoclinic connections under variation of one parameter is based on continuation methods and allows us to detect all known codimension 1 and 2 bifurcations in three-dimensional (3D) maps, including tangencies and generalized tangencies. MatContM provides a graphical user interface, enabling interactive control for all computations. As the prime new feature, we discuss an algorithm for initializing connecting orbits in the important special case where either the stable or unstable manifold is one-dimensional, allowing us to compute all homoclinic orbits to saddle points in 3D maps. We illustrate this algorithm in the study of the adaptive control map, a 3D map introduced in 1991 by Frouzakis, Adomaitis, and Kevrekidis, to obtain a rather complete bifurcation diagram of the resonance horn in a 1:5 Neimark-Sacker bifurcation point, revealing new features.

CCS Concepts: • **Mathematics of computing** → **Mathematical software**; **Numerical analysis**; *Solvers*; Computations on matrices;

Additional Key Words and Phrases: Iterated map, homoclinic orbit, bifurcation, MatContM

1 INTRODUCTION

We consider dynamical systems generated by smooth nonlinear maps,

$$x \mapsto f(x, \alpha), \quad x \in \mathbb{R}^n, \ \alpha \in \mathbb{R}^m, \tag{1}$$

Authors' addresses: N. Neirynck and W. Govaerts, Ghent University, Dept. Appl. Maths, Comp. Sci. and Stats, Krijgslaan 281, S9, 9000 Ghent, Belgium; emails: {Niels.Neirynck, Willy.Govaerts}@UGent.be; Y. A. Kuznetsov, Utrecht University and University of Twente, Budapestlaan 6, Dept. of Maths 3584 CD Utrecht, Netherlands; email: I.A.Kouznetsov@uu.nl; H. G. E. Meijer, University of Twente, Maths and Comp. Sci., Zilverling 3016, PO Box 217, Enschede, Netherlands; email: h.g.e@meijer.utwente.nl.

with state variable x and parameter α. The Kth iterate of Equation (1) at parameter value α is defined by

$$x \mapsto f^{(K)}(x, \alpha) = \underbrace{f(f(\cdots f(x, \alpha), \cdots, \alpha), \alpha)}_{K \; times}. \tag{2}$$

Bifurcation analysis usually starts with *fixed points* $x \in \mathbb{R}^n$, where $f(x, \alpha) = x$. Cycles (periodic orbits) of maps are studied as fixed points of $f^{(K)}$.

A sequence $(x_k)_{k \in \mathbb{Z}}$ is called a *connecting orbit* of f if

$$\begin{aligned} \lim_{k \to -\infty} x_k &= x_{-\infty}, \\ f(x_k, \alpha) &= x_{k+1}, \quad \forall k \in \mathbb{Z}, \\ \lim_{k \to +\infty} x_k &= x_{+\infty}, \end{aligned} \tag{3}$$

where $x_{-\infty}$ and $x_{+\infty}$ are (necessarily) fixed points of f. The connecting orbit is called *homoclinic* if $x_{+\infty} = x_{-\infty}$ and *heteroclinic* otherwise. From a geometric point of view, the connecting orbit lies in the intersection of the unstable manifold $W^u(x_{-\infty})$ of $x_{-\infty}$ and the stable manifold $W^s(x_{+\infty})$ of $x_{+\infty}$. These manifolds are defined as

$$W^s(x_{+\infty}) = \left\{ x \in \mathbb{R}^n : f^{(J)}(x, \alpha) \to x_{+\infty} \text{ as } J \to +\infty \right\} \tag{4}$$

and

$$W^u(x_{-\infty}) = \left\{ x \in \mathbb{R}^n : \exists \{q_k\}, q_0 = x \text{ and } f(q_{k+1}, \alpha) = q_k, \text{ and } \lim_{k \to \infty} q_k = x_{-\infty} \right\}. \tag{5}$$

This observation leads to a method for computing connecting orbits for planar maps. Algorithms exist for computing one-dimensional stable and unstable manifolds. First discussed in References [22] and [8], the algorithms "grow" manifolds by repeatedly adding points and so collect piecewise linear approximations to the manifolds. By intersecting these computed stable and unstable manifolds, one obtains connecting orbits. The result is shown in Figure 1 for the Generalized Hénon Map [14]:

$$\begin{pmatrix} x \\ y \end{pmatrix} \mapsto \begin{pmatrix} y \\ \alpha - \beta x - y^2 + Rxy + Sy^3 \end{pmatrix}. \tag{6}$$

The parameters are α, β, R, and S.

Figure 1 depicts a computed part of a homoclinic orbit of Equation (6). There are infinitely many points between point 1 and the fixed point (green cross), leaving the fixed point through the unstable manifold (red line). There are also infinitely many points between point 10 and the fixed point, converging to the fixed point through the stable manifold (blue line). Close to the fixed point, the stable and unstable manifolds may be approximated by the stable and unstable eigenspaces. So, an orbit piece approximates a connecting orbit if the endpoints are sufficiently close to the fixed point and lie within the stable and unstable eigenspaces. The endpoints are chosen sufficiently close to the fixed point so that the stable and unstable manifolds can be accurately approximated by the stable and unstable eigenspaces, respectively. The mathematical conditions that express that the first and last endpoints are in the unstable and stable eigenspaces, respectively, are called the boundary conditions. A set of mathematical conditions can now be used to continue a connecting orbit in a system with a state space of any dimension. The conditions form a set of Equations [20] that can be used to either improve an approximately given connecting orbit using Newton's method, or to continue the orbit when a system parameter is freed.

With respect to Figure 1, we note that more homoclinic orbits exist, since every intersection point of the stable and unstable manifolds gives rise to a homoclinic orbit. For example, Figure 2 shows another, so-called secondary, homoclinic connection. We note that it "goes around" twice.
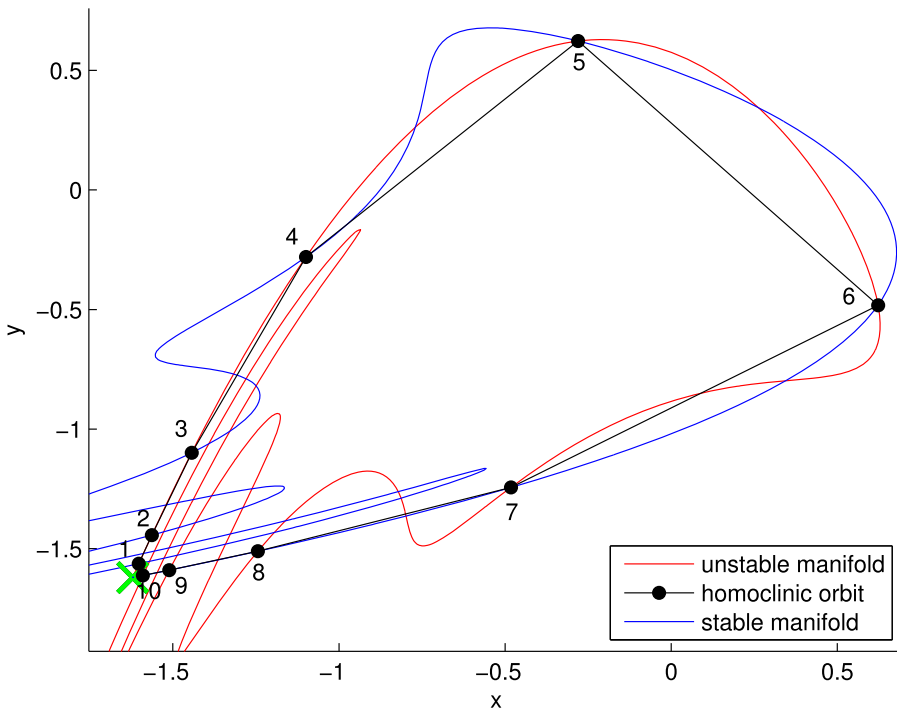
Fig. 1. One-dimensional stable (blue) and unstable (red) manifolds in a saddle fixed point (green cross) of the Generalized Hénon map. By using some intersection points between the two manifolds we obtain a homoclinic orbit (black) of that saddle. The parameter values are $\alpha = -0.4$, $\beta = 1.03$, $R = -0.1$ and $S = 0$. The fixed point is $(-1.6211, -1.6211)^T$.

Algorithms for numerical continuation of connecting orbits of maps have been proposed and analysed [3] and implemented within the continuation packages AUTO [26] and MatContM [20]. Similar codes were known to experts in the 1980s; see References [18, 23]. These methods provide defining systems that the connecting orbit satisfies. All these codes have proven their usefulness, but they have one major drawback, the initial data. While, for cycles, these can be found by simulation, this is a nontrivial task for connecting orbits, or requires insight into the model [17, 27]. A simulation may suggest a connecting orbit to be present but does not guarantee for its existence nor does it provide a good starting seed. In Reference [26], such initial data was constructed by generating an orbit from a one-dimensional (un)stable manifold of a saddle and then applying a secant method. The method assumes that the connecting orbit exists for the given parameter values. For planar maps the common practice is to first compute the one-dimensional manifolds and then to determine intersection points. Here, we generalize these ad hoc approaches to a systematic initialization procedure based on the computation of one-dimensional invariant manifolds. While this is not sufficient in all dimensions, it covers all three-dimensional cases.

During numerical continuation, the connecting orbit may undergo a bifurcation. The typical case is a tangency where two, so-called primary, connecting orbits coalesce and disappear much like the common saddle-node bifurcation. Indeed, the test-function for the tangency is analogous to the saddle-node case. Several other codim 1 and 2 cases for homoclinic orbits have been studied theoretically, see, e.g., References [12, 13], and numerically explored, see, e.g., References [11, 13],
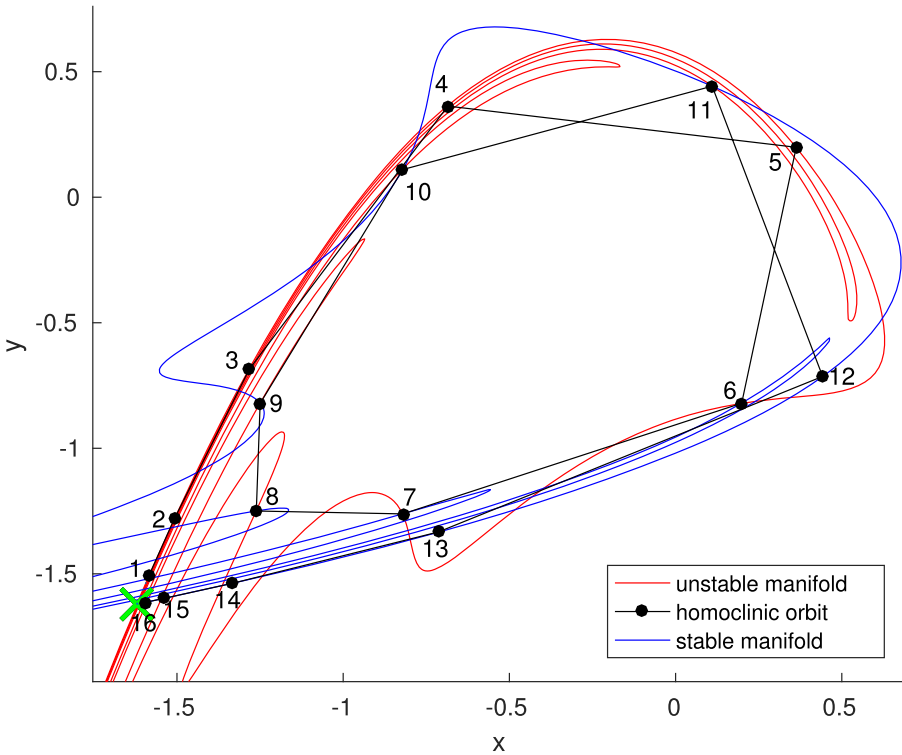
Fig. 2. By using other intersection points in Figure 1 another homoclinic orbit is obtained.

and related references. The conditions for these bifurcations are related to either the multipliers of the saddle-cycle and/or the geometry of the connecting orbit. The existing numerical continuation codes, however, do not detect these cases. Here, we also provide test-functions to detect these codim 1 and 2 bifurcations of connecting orbits during continuation.

1.1 Overview

In Section 2, we discuss the algorithms for growing one-dimensional stable and unstable manifolds in multidimensional spaces as now implemented in MatContM. The stable manifold computation is in the multidimensional case based on ideas of C. Bruschi and F. Della Rossa (personal communication). In Section 3, we discuss the initialization of homoclinic orbits of a map from a one-dimensional stable or unstable manifold. In Section 4, codimension 1 and 2 bifurcations of homoclinic orbits are discussed, including the use of test functions for their detection in the numerical continuation algorithms of MatContM.

   After a brief introduction to MatContM in Section 5, we present in Section 6 an extensive case study of the adaptive control map proposed in Reference [10] and studied in Reference [9]. This involves initialization of homoclinic orbits, numerical continuation of homoclinic orbits and tangencies and the detection of codimension 2 bifurcations of homoclinic orbits. Finally, we study with MatContM the full resonance horn in a 1:5 Neimark-Sacker bifurcation of the map, including tangencies of heteroclinic connections and other global bifurcation phenomena.

2 GROWING ONE-DIMENSIONAL STABLE AND UNSTABLE MANIFOLDS

2.1 One-Dimensional Unstable Manifolds

To compute one-dimensional unstable manifolds, we use a slightly improved version of the algorithm described in Reference [22] (the improvement is mainly in a better bookkeeping of the metadata of the algorithm). The algorithm starts with a saddle fixed point. Near the fixed point, the algorithm uses the unstable eigenspace (which is assumed to be one-dimensional) to approximate the unstable manifold.

Two issues must be kept in mind. First, both directions along the unstable manifold can possibly lead to a connecting orbit and should be tried. Second, if the unstable multiplier is negative, then the second iterate of the map is automatically used. This ensures that we use an orientation preserving map, a necessary condition for the algorithm.

The first part is to choose a point in the unstable eigenspace close to the saddle point and add points along the unstable manifold by applying the map. This procedure is applied as long as the distance between two consecutive points is within some interval and an angle condition is satisfied.

The main part consists of adding new points in the direction away from the fixed point that are at each step at most a prescribed distance from the last added point. The distance changes from step to step with the curvature of the manifold; many points are added when encountering sharp folds while few points are added during locally straight lines. To avoid cutting of sharp folds, a restriction is placed on the angle of the new point and the last two points. Our implementation of this algorithm (an adaptation of the implementation in Reference [20]) also keeps track of the segment of the manifold approximation that contains the preimage of each newly added point.

2.2 One-Dimensional Stable Manifolds

England et al. [8] describe an algorithm for growing one-dimensional stable manifolds for planar maps in which the inverse is not explicitly or implicitly (i.e., by a Newton-like iteration) used. However, their approach, called circle search, does not generalize to higher-dimensional spaces. We therefore use a slightly improved version of an algorithm by C. Bruschi, which essentially uses the inverse in the form of Newon-like iterations, implicitly assuming that the manifold is locally unique (the improvement is mainly in a better bookkeeping of the metadata of the algorithm). The algorithm starts with a saddle fixed point. Near the fixed point, the algorithm uses the stable eigenspace (which is assumed to be one-dimensional) to approximate the stable manifold.

The same issues as for unstable manifolds must be kept in mind.

In the first part of the algorithm, we choose a point in the stable eigenspace sufficiently close to the saddle point and add points along the stable manifold in the direction toward the fixed point by applying the inverse map (implicitly, by Newton iteration), as long as the distance between two points is below a threshold and an angle condition is satisfied.

The main part consists of adding new points in the direction away from the fixed point, which are at each step at a distance approximately equal to or smaller than δ_k, which is one of the threshold parameters in the code. Let p_{end} be the last computed point on the stable manifold.

The first step of the procedure is sketched in Figure 3. It is first checked that $\|f^{-1}(p_{end}) - p_{end}\| > \delta_k$, where $f^{-1}(p_{end})$ is computed by Newton iterations. If this is not the case, then δ_k is decreased. Next, by tracing back the computed points along the stable manifold two consecutive points q_L and q_R are identified such that $\|f^{-1}(q_R) - p_{end}\| > \delta_k$ and $\|f^{-1}(q_L) - p_{end}\| < \delta_k$. In the process, $p_R = f^{-1}(q_R)$ and $p_L = f^{-1}(q_L)$ are identified. It is not excluded that $p_L = p_{end}$.
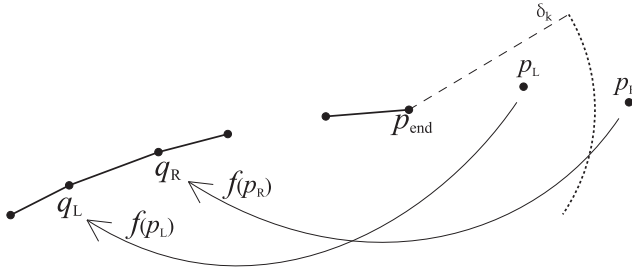
Fig. 3. Computing a new point on the stable manifold: first step. The dotted arc represents a sphere of radius δ_k around p_{end}. This figure is adapted from a figure by C. Bruschi.
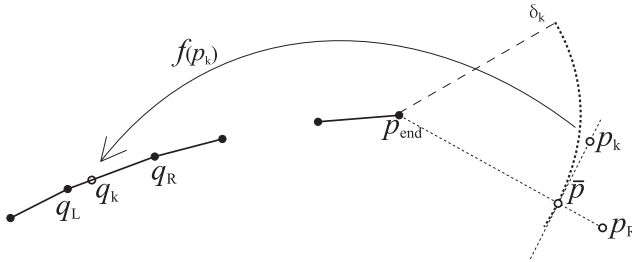

Fig. 4. Computing a new point on the stable manifold: second step. This figure is adapted from a figure by C. Bruschi.

Next, the zero-order approximation $\bar{p}$ to the sought next point p_k on the stable manifold is computed as

$$\bar{p} = p_{end} + \delta_k \frac{p_R - p_{end}}{\|p_R - p_{end}\|};$$

see Figure 4. The further aim is to obtain p_k as the solution to the system that consists of

$$f(p_k) = q_L + \tau(q_R - q_L) \tag{7}$$

and

$$\langle p_k - \bar{p}, \bar{p} - p_{end} \rangle = 0. \tag{8}$$

The geometric meaning of these conditions is clear from Figure 4. Together, Equations (7) and (8) constitute a system of $n + 1$ equations in $n + 1$ variables, namely the components of p_k and the scalar τ, where n is the dimension of the state space. To obtain a first-order approximation of (p_k, τ), we solve the linearized system

$$\begin{bmatrix} J|_{\bar{p}} & -q_R + q_L \\ (\bar{p} - p_{end})^T & 0 \end{bmatrix} \begin{bmatrix} p_k \\ \tau \end{bmatrix} = \begin{bmatrix} q_L - f(\bar{p}) + J|_{\bar{p}}\bar{p} \\ (\bar{p} - p_{end})^T \bar{p} \end{bmatrix}, \tag{9}$$

which is equivalent to a single Newton step, starting with $(\bar{p}, 0)^T$ as initial guess.

It turns out that in many cases the Jacobian matrix of the system Equations (7) and (8) is ill-conditioned at the solution point. Therefore, in practice, we keep τ fixed and solve Equation (7) by a Newton iteration. The code contains several further checks, e.g., an angle condition (to handle the case of sharp fold points) and the requirement that τ is positive and smaller than a chosen threshold. If one of these requirements is not satisfied, then δ_k is decreased and the process is started again.

3 INITIALIZATION OF A HOMOCLINIC ORBIT FROM A ONE-DIMENSIONAL MANIFOLD

3.1 Initialization from a One-Dimensional Unstable Manifold

Logically, four parts can be distinguished in the initialization algorithm. We discuss them separately.

3.1.1 Growing the Unstable Manifold. We use the algorithm described in Section 2.1 to obtain an unstable one-dimensional manifold.

3.1.2 Intersecting the Stable Eigenspace. If a point on the unstable manifold also lies on the stable manifold of $x_{\pm\infty}$, then it is a point of a connecting orbit. However, computing manifolds of dimension higher than one is a difficult problem; it is practically unfeasible if the dimension is higher than two, but see Reference [25] for recent advances. We avoid this difficulty by only considering the stable eigenspace near $x_{\pm\infty}$. If an intersection point of the unstable manifold with the stable eigenspace is close enough to $x_{\pm\infty}$, then it serves as an approximation of an intersection point with the stable manifold. To find intersection points with the stable eigenspace, we consider a left eigenvector v_u^l of the (unique) unstable eigenvalue. The inner product function with v_u^l generically changes sign when the unstable manifold crosses the stable eigenspace and the exact intersection point is approximated by a linear interpolation in the line segment where the sign change happens.

3.1.3 Tracing Back the Orbit to $x_{-\infty}$. The intersection point P found in Section 3.1.2 is only an approximation to a point on the homoclinic orbit and needs corrections by a Newton method applied to a defining system, which is a truncation of Equation (3) with projection boundary conditions, as discussed in Reference [20]. This orbit has to be approximated first. We start with the segment information to trace back the orbit:

First, we locate the segment on the piecewise linear approximation that contains the point P. This segment is a line, defined by two points P_1 and P_2. These points were added at some stage by the algorithm. We retrieve two segments, one that contains the preimage of P_1 and one that contains the preimage of P_2. These two segments can be the same, they can be consecutive or there can be several segments between them. The preimage of P lies on one of these segments. Bisection is applied on these segments to find an accurate value for the preimage of P. Once the preimage of P has been located, we repeat the process with the preimage as the new P.

At some stage, we have traced the orbit back to the part of the manifold approximation where points were added along the unstable eigenspace during the initial phase. We can then decide to stop or add extra points. For continuation purposes, we need to get sufficiently close to the fixed point.

3.1.4 Adding Points Toward $x_{+\infty}$. The computation of the unstable manifold is usually quite time-consuming and the computation of each subsequent intersection point with the stable eigenspace requires more effort. At some stage, we have to decide that we are close enough to the stable manifold. We then add new points simply by applying the map and then projecting back on the stable eigenspace to avoid being thrown off due to the presence of the unstable direction.

3.2 Initialization from a One-Dimensional Stable Manifold

Essentially, this is done like in the case of an unstable manifold. Two other issues have to be taken into account. First, tracing back the orbit is simpler in this case, since we can apply the map and then project to the corresponding segments of the already computed stable manifold and choose
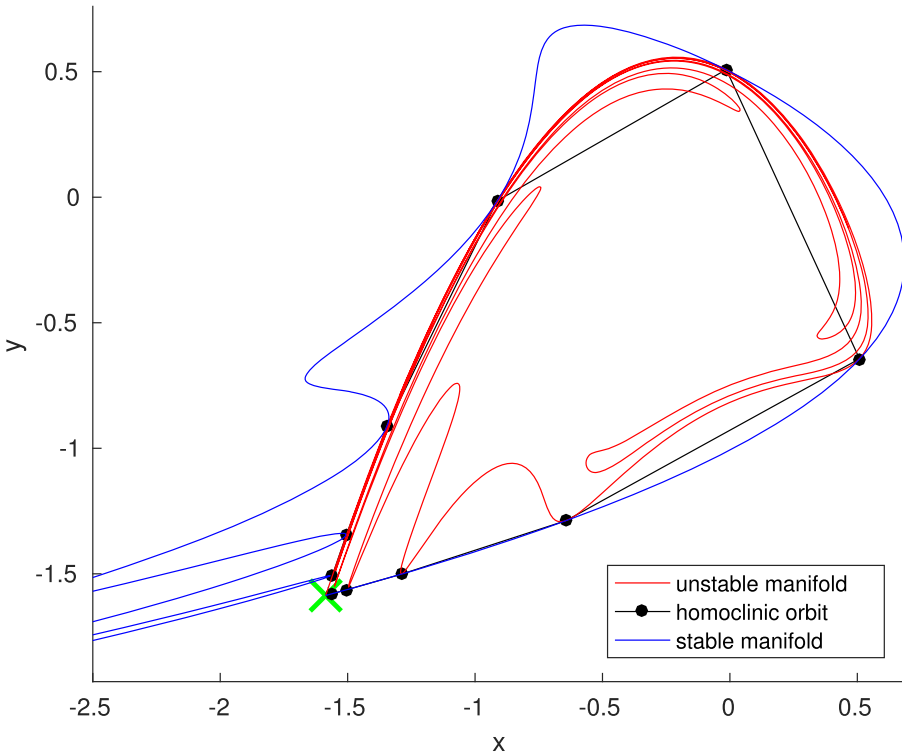
Fig. 5. A tangency detected during the continuation of the homoclinic orbit depicted in Figure 1 with β as the free parameter. The tangency is found for $\beta = 0.999974$.

the closest point. Second, adding points to $x_{-\infty}$ is now done by applying the inverse map (in the form of a Newton iteration procedure) and project to the unstable eigenspace.

4 DETECTION AND CONTINUATION OF BIFURCATIONS

Once a connecting orbit is computed, one can continue it under variation of a parameter. Figure 5 shows how during the continuation of the homoclinic orbit depicted in Figure 1 with β as the free parameter, we detect a tangency (limit point, LP_HO in figure 6) for $\beta = 0.999974$. The stable and unstable manifolds associated with the tangency are displayed in Figure 5. The stable manifold (blue) and the unstable manifold (red) are tangential to each other in every intersection point.

In Figure 6, we display the relation graph between a general homoclinic orbit (HO, at the top), some codimension 1 bifurcations (HO_NS, HO_Dx and LP_HO at the second line) and codimension 2 bifurcations (HT_NS, HT_Dx, HT_xF and HT_Ex at the bottom line).

In this graph "HO" stands for "Homoclinic Orbit," "HT" for "Homoclinic Tangency," "NS" for "Neutral Saddle," "D" for "Double," "LP" for "Limit Point," "E" for "Extended," "F" for "Foliation," and "x" for either "S" (Stable) or "U" (Unstable). We note that a limit point of homoclinic orbits is called a homoclinic tangency, so in this graph "LP_HO" and "HT" are used interchangeably.

The scenario for detecting bifurcations is generic: on a computed curve of bifurcation points with codimension i one detects bifurcations with codimension $i + 1$ by monitoring test functions that change sign at the occurrence of such higher codimension points. These test functions are
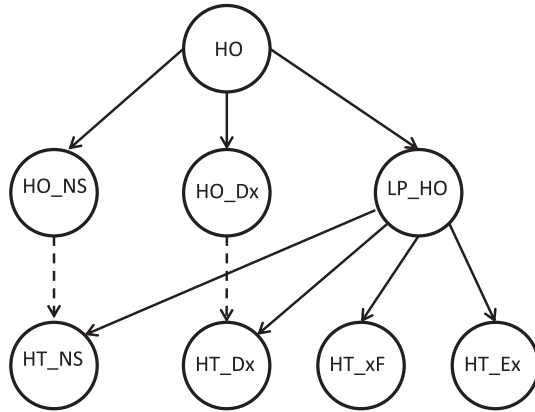
Fig. 6. Detection graph of homoclinic bifurcations. "x" stands either for S (stable) or U (unstable). Dashed curves indicate that such a bifurcation exists, but its detection is not supported.

evaluated at each step during the continuation. When a sign change is detected, a bisection-like algorithm is used to locate the higher-codimension bifurcation.

4.1 Codimension 1 Bifurcations

Let n_s, n_c, n_u be the number of stable, critical, and unstable multipliers of the fixed point of a homoclinic orbit, respectively, i.e., those with modulus less than 1, equal to 1, and larger than 1, respectively. Also, let $\mu_1^s, \mu_2^s, \ldots, \mu_{n_s}^s$ be the stable multipliers, ordered by decreasing modulus. Similarly, let $\mu_1^u, \mu_2^u, \ldots, \mu_{n_u}^u$ be the unstable multipliers, ordered by increasing modulus. The multipliers μ_1^s and μ_1^u are called the leading stable and unstable multipliers, respectively. Also, let $(x^1, x^2, \ldots, x^N)$ be the computed part of a homoclinic orbit.

4.1.1 Neutral Saddle Homoclinic Orbit HO_NS. This is the case where $n_c = 0$ and $|\mu_1^s \mu_1^u| = 1$. The test function is defined as $\phi_{NS} = |\mu_1^s \mu_1^u| - 1$.

4.1.2 Double-Stable Homoclinic Orbit HO_DS. This is the case where $n_c = 0$ and $\mu_1^s = \mu_2^s$. The test function ϕ_{DS} is defined as $(\mu_1^s - \mu_2^s)^2$ in the case where both μ_1^s and μ_2^s are real, as $-(\mathfrak{I}(\mu_1^s - \mu_2^s))^2$ if they form a conjugate complex pair, and undefined in all other cases.

4.1.3 Double-Unstable Homoclinic Orbit HO_DU. This is the case where $n_c = 0$ and $\mu_1^u = \mu_2^u$. The test function ϕ_{DU} is defined as $(\mu_1^u - \mu_2^u)^2$ in the case where both μ_1^u and μ_2^u are real, as $-(\mathfrak{I}(\mu_1^u - \mu_2^u))^2$ if they form a conjugate complex pair, and undefined in all other cases.

4.1.4 Homoclinic Tangency LP_HO. This is the case of a limit point of homoclinic orbits. The test function is simply the parameter component of the tangent vector to the curve of approximate homoclinic orbits.

4.2 Codimension 2 Bifurcations

The following codimension 2 bifurcations occur when in a tangency another condition is satisfied.

4.2.1 Neutral Saddle Homoclinic Tangency HT_NS. This is the case where $n_c = 0$ and $|\mu_1^s \mu_1^u| = 1$. The test function is $\phi_{NS} = |\mu_1^s \mu_1^u| - 1$.
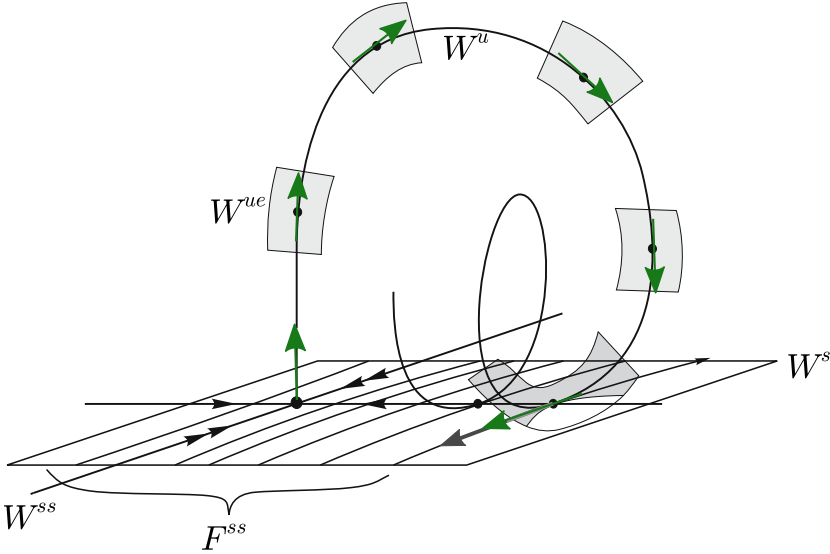
Fig. 7. An instance of a HT_SF bifurcation. The green arrows are the tangent vectors of the unstable manifold. W^s, W^u, W^{ss}, and W^{ue} denote the stable, unstable, strongly stable, and unstable-extended manifolds, respectively. F^{ss} is the strongly stable foliation. Upon returning in the stable manifold the tangent vectors are tangential to the strongly stable foliation. The Figure is adapted from Reference [13].

4.2.2   Double-Stable Homoclinic Tangency HT_DS. This is the case where $n_c = 0$ and $\mu_1^s = \mu_2^s$. The test function ϕ_{DS} is defined as $(\mu_1^s - \mu_2^s)^2$ in the case where both μ_1^s and μ_2^s are real, as $-(\Im(\mu_1^s - \mu_2^s))^2$ if they form a conjugate complex pair, and undefined in all other cases.

4.2.3   Double-Unstable Homoclinic Tangency HT_DU. This is the case where $n_c = 0$ and $\mu_1^u = \mu_2^u$. The test function ϕ_{DU} is defined as $(\mu_1^u - \mu_2^u)^2$ in the case where both μ_1^u and μ_2^u are real, as $-(\Im(\mu_1^u - \mu_2^u))^2$ if they form a conjugate complex pair, and undefined in all other cases.

4.2.4   Stable Foliation Homoclinic Tangency HT_SF. Gonchenko, Gonchenko and Tatjer [13] studied the dynamics due to a generalized homoclinic tangency for maps. This generalized tangency is defined as a tangency of the unstable manifold to the strongly stable foliation of the stable manifold at the homoclinic orbit. Hence, this bifurcation may occur in (at least) three-dimensional maps, and we restrict to the case where the unstable manifold is one-dimensional. Then, for neighborhoods of the connecting orbit, there exist return maps for each sufficiently large iteration number such that the dynamics on this neighborhood is given by a Generalized Hénon Map. See Figure 7 for a sketch of the orbit structure.

The construction of the test function ϕ_{SF} is based on the observation that in a generalized homoclinic tangency, the tangent vector to the unstable manifold near the saddle is orthogonal to the leading stable left eigenvector v_s^l, which we assume to be real.

The tangent vector along the unstable manifold during continuation of a homoclinic tangency is not available as only the homoclinic orbit and not the full manifold is computed during continuation. We therefore need to approximate the tangent vector of the unstable manifold. We start with the unstable eigenvector v_u at the saddle point. Let the computed internal points of the homoclinic orbit (different from the saddle point) be denoted by $x_1, x_2, \ldots, x_N$ in that order. Also, let $v_u^1, v_u^2, \ldots, v_u^N$ be the corresponding tangent vectors to the unstable manifold. Now as tangent
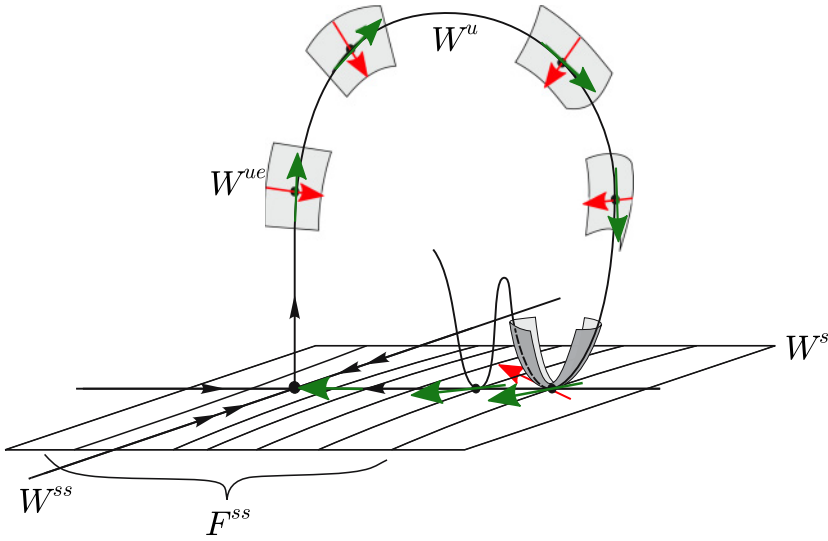
Fig. 8. An instance of a HT_ES bifurcation. W^s, W^u, W^{ss}, and W^{ue} denote the stable, unstable, strongly stable, and unstable-extended manifolds, respectively. F^{ss} is the strongly stable foliation. The red arrows are mapped from the leading stable eigenvector at the saddle point. Together with the tangent vectors of the unstable manifold, they span the tangent plane to the W^{ue} manifold. Upon returning in the stable manifold the unstable-extended manifold becomes tangential to the stable manifold. The tangent vector to the unstable manifold (green arrow) converges to a vector in the leading stable direction. The Figure is adapted from Reference [13].

vectors are mapped to tangent vectors by the linearization, i.e., $v_u^{m+1} \approx D_f(x_m)v_u^m$, we can map v_u along the connecting orbit so that the tangent vector at the unstable manifold at any point x_m of the connecting orbit is given by

$$v_u^m = D_f(x^{m-1})D_f(x^{m-2})\cdots D_f(x^1)v_u.$$

Then, we can choose $\phi_{SF} = v_s^{l\,T}v_u^N$ as a test function.

4.2.5 Extended Stable Homoclinic Tangency HT_ES. In the case of a one-dimensional unstable manifold the unstable extended manifold W^{ue} depicted in Figure 8 is a non-unique invariant manifold that contains the unstable manifold and the leading (assumed to be real) stable manifold. Its tangent plane at each orbit point x_m is spanned by the tangent vector v_u^m to the unstable manifold (the green arrow in Figure 8) and the mapped leading stable eigenvector v_s^m (the red arrow in Figure 8), which is assumed to be real. The HT_ES bifurcation occurs if the unstable extended manifold is tangential to the stable manifold. Since v_u^m is already tangential to the stable manifold, the condition is that v_s^m is also tangential to the stable manifold, i.e., orthogonal to the left unstable eigenvector at the saddle point v_u^l. As in the preceding case this bifurcation may occur in (at least) three-dimensional maps. The test function ϕ_{ES} is defined in a dual way to ϕ_{SF} and given by $\phi_{ES} = v_u^{l\,T}v_s^N$ where v_s^N is defined as in the previous case, replacing v_u by the leading stable eigenvector v_s.

4.2.6 Unstable Foliation Homoclinic Tangency HT_UF. This generalized tangency is defined as a tangency of the stable manifold to the stronly unstable foliation of the unstable manifold at the homoclinic orbit. Hence, this bifurcation may occur in (at least) three-dimensional maps, and

we restrict to the case where the stable manifold is one-dimensional and the leading unstable eigenvalue is real and unique. So, the tangent vector to the stable manifold near the saddle is orthogonal to the leading unstable left eigenvector v_u^l.

We map v_s along the connecting orbit so that the tangent vector at the stable manifold at x_m is given by

$$v_s^m = D_f^{-1}(x^{m+1})D_f^{-1}(x^{m+2})\cdots D_f^{-1}(x^N)v_s.$$

Then, we choose $\phi_{UF} = v_u^{l\,T}v_s^1$ as a test function.

4.2.7 Extended Unstable Homoclinic Tangency HT_EU. As in the preceding case this bifurcation may occur in (at least) three-dimensional maps, and we restrict to the case where the stable manifold is one-dimensional and the leading unstable eigenvalue is real and unique.

The test function ϕ_{EU} is defined in a dual way to ϕ_{UF} and given by $\phi_{EU} = v_s^{l\,T}v_u^1$, where v_u^1 is defined as in the preceding case.

5   THE BASICS OF THE USE OF MATCONTM

The numerical bifurcation analysis of Equation (1) requires a dedicated software package. A MAT-LAB continuation toolbox MatContM, available at *http://sourceforge.net/projects/matcont/*, was developed for this purpose; see also References [15], [16], and [19].

The "M" in MatContM stands for "maps." The site indeed also contains MatCont [7], a toolbox that provides numerical continuation software for the bifurcation study of ODEs.

MatContM detects and locates fixed points and cycles in one parameter, detects codimension 1 bifurcations, continues bifurcation curves in two parameters, and detects codimension 2 bifurcation points. Computation of orbits and Lyapunov exponents is also implemented. As in MatCont a Moore-Penrose variant of pseudo-arclength continuation is used to approximate these curves; see References [24] and [7]. Bifurcations are detected by encountering zeros of test functions during the continuation process.

Critical normal form coefficients are computed at bifurcation points. For this, we rely on symbolic derivatives or if these are not available, on automatic differentiation. Bifurcation curves are defined by a system of equations consisting of fixed point and bifurcation conditions. With one free parameter, we have curves of fixed points, cycles and connecting orbits. With two free system parameters, we can compute curves of limit points, period-doubling and Neimark-Sacker points, homoclinic and heteroclinic tangencies of manifolds.

The continuation curves can be visualized using the plot capabilities of the GUI; this can be done during and after the continuation. Special windows are provided to help with maintaining systems, diagrams and curves when generating a large amount of data. In Reference [21] this software is extensively used to study the bifurcation behavior of fixed points and cycles in biological models. This software was also used in a study of resonance tongues in Reference [16] and in the analysis of an economic model in Reference [1].

6   CASE STUDY: ADAPTIVE CONTROL MAP

The map

$$f : \begin{pmatrix} x \\ y \\ z \end{pmatrix} \mapsto \begin{pmatrix} y \\ bx + k + zy \\ z - \frac{ky}{c+y^2}(bx + k + zy - 1) \end{pmatrix} \tag{10}$$

was introduced in Reference [10] and studied in Reference [9]. The parameters are k, b, and c. In Reference [9], we find an example of a subcritical period-5 resonance horn. Near the tip of the
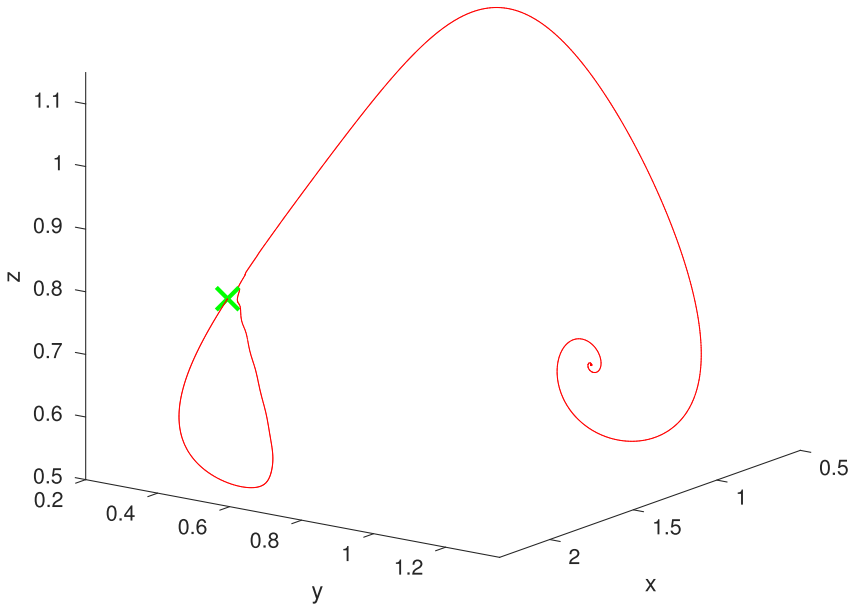
Fig. 9. The unstable manifold (red curve) of the saddle (green cross) of the fifth iterate of Equation (10). The unstable manifold moves back toward the saddle and then away from the saddle toward another fixed point.

horn, the authors detect and compute a homoclinic tangency curve. This tangency curve is shown in the (k, b) parameter space, the parameter c is kept at 0.1.

We will use the algorithms in Sections 2 and 3 to compute a homoclinic orbit and recompute the homoclinic tangency curve in Reference [9] in more detail using continuation methods.

For $(k, b) = (0.824, -0.47)$, we obtain a saddle of $f^{(5)}$ near $(1.56, 0.25, 0.72)^T$ using Newton's method on $f^{(5)}(X) - X = 0$. The saddle values are $x = 1.566650994666793$, $y = 0.253929996002914$, $z = 0.725117829106035$. The multipliers of this saddle are 0.0674, 0.1957 and 1.7483, so we have a one-dimensional unstable manifold and a two-dimensional stable manifold.

We use our algorithm to find a homoclinic orbit. We start this by growing the unstable manifold, following the procedure in Section 2.1. The resulting unstable manifold is shown in Figure 9 as the red line that emanates from the saddle, then advances back toward it while showing slight oscillations before receding and moving on. This indicates that we are nearby a homoclinic connection.

The second step is to intersect the stable eigenspace as described in Section 3.1.2. The tangent plane is shown in Figure 10 as the grey plane. We intersect this plane with the unstable manifold (red) and take the point that is closest to the saddle (green cross). The third step is taking preimages of this point in the unstable manifold (blue crosses in Figure 10), as described in Section 3.1.3. This backward computation of the homoclinic orbit ends when we are close enough to the saddle. The fourth step is adding points at the stable side of the homoclinic orbit. For this, we use the method described in Section 3.1.4. This is shown in Figure 10, where we start from the initial intersection point (green cross) and add new points (magenta crosses).

This approximation of a homoclinic orbit is a sufficiently accurate seed for Newton's method with the defining system mentioned in Section 1.

Initial Newton corrections are always applied in MatContM when starting a continuation, so we can use the suboptimal approximation as the initial orbit for a homoclinic continuation. We select k as the free parameter. Figure 11 shows the approximation to the homoclinic orbit when
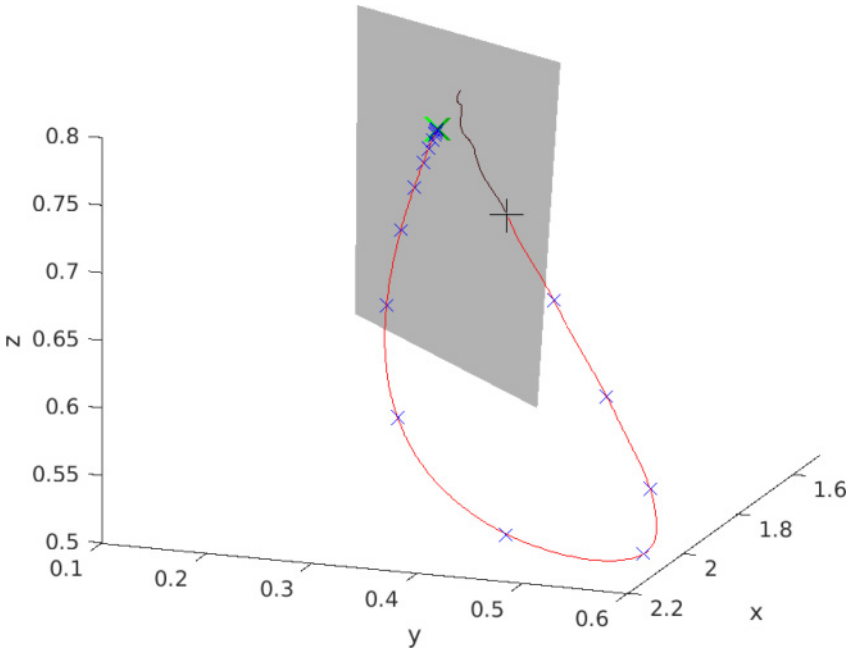
Fig. 10. The unstable manifold (red line), the stable eigenspace (grey plane), their intersection point closest to the saddle (black +), points of the approximate homoclinic orbit by computing preimages (blue crosses).
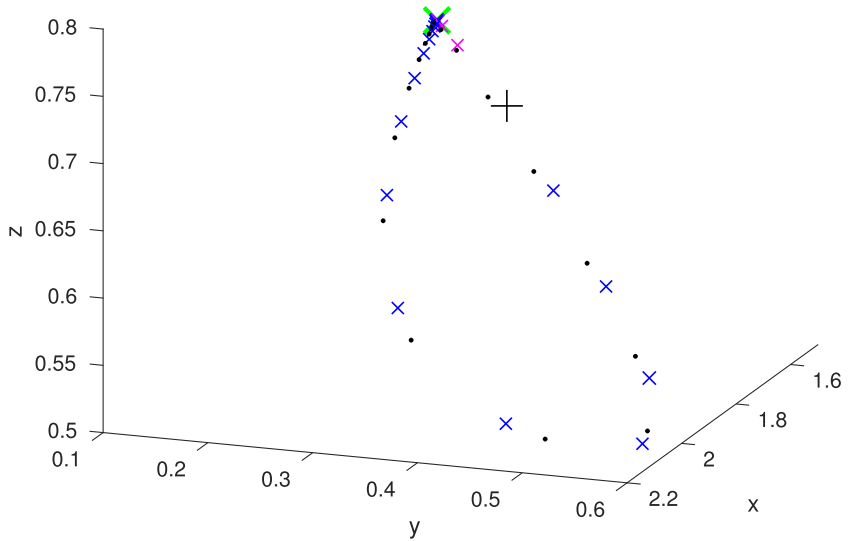

Fig. 11. The approximation obtained by our algorithm (cf. Figure 10) where additional points are added between the intersection point and the saddle (magenta crosses) and a corrected orbit using Newton's method (black dots). This corrected orbit is the starting point in a homoclinic connection continuation.
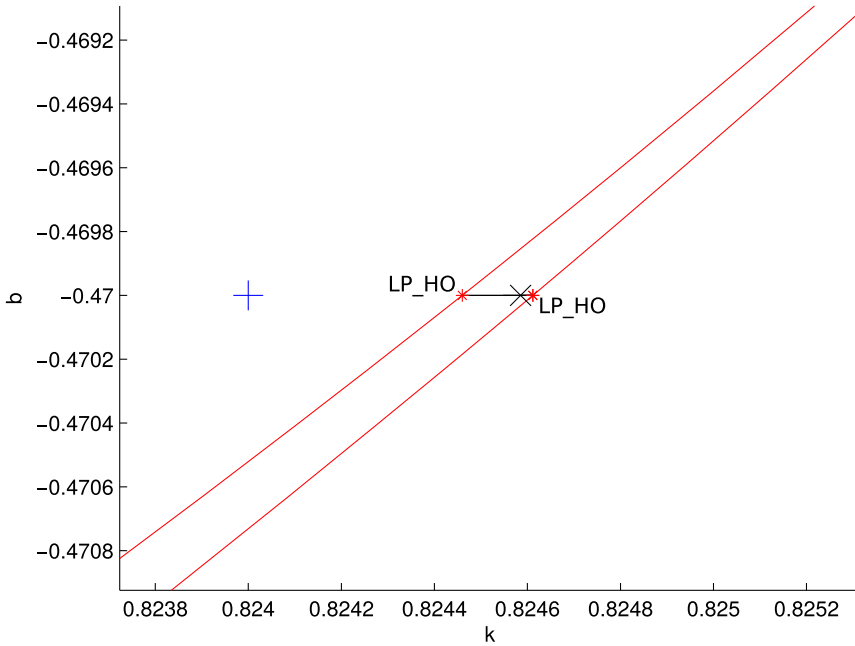
Fig. 12. The approximation is represented by the blue +. The corrected orbit is represented by the black cross. The corrected orbit is the first point in a homoclinic connection continuation, the black line. During this continuation, two homoclinic tangencies are detected, labeled by LP_HO (limit point of a homoclinic orbit). The red lines are part of homoclinic tangency continuations started from both LP_HO points. Homoclinic connections exist between those two red curves.

our algorithm is applied to the data presented in Figure 10 and an orbit obtained after Newton corrections by varying the parameter k, as done by MatContM.

Figure 12 shows the correction in the (k, b) parameter space and the continuation of the homoclinic connection by varying the parameter k. This is depicted by a black line emanating from the corrected orbit. We encounter two distinct homoclinic tangencies during the continuation. These tangencies are limit points of the homoclinic connection curve and therefore denoted as LP_HO (Limit Point of a Homoclinic Orbit). The continuation moves back and forth between these two tangencies several times.

From both homoclinic tangencies, we start homoclinic tangency continuations in both directions using k and b as free parameters. The curves of homoclinic tangencies are seen in Figure 12 as red curves. Robust homoclinic connections exist between those two red lines. This reveals that our starting point for obtaining an approximation was poorly chosen, since there was no homoclinic connection. Choosing a saddle near homoclinic connections can thus suffice to obtain a homoclinic connection for continuation. This is very useful, since areas in the parameter space where connecting orbits exist are usually very narrow.

Here, we provide a much more detailed picture filling in gaps in Reference [9]. Figure 13 extends Figure 12 and shows the full result of both homoclinic tangency continuations. The black curve containing the two tangencies from Figure 12 is marked on Figure 13 using a black +. In one direction the red tangency curves move toward the upper Resonance 1:1 (R1) point where the continuation process encounters convergence problems. Figure 14 shows homoclinic tangencies in phase space on the left red line in Figure 12. The blue orbit is the initial homoclinic tangency for $k = 0.82445996$, $b = -0.47$. The smallest red one is closest to the R1 point.
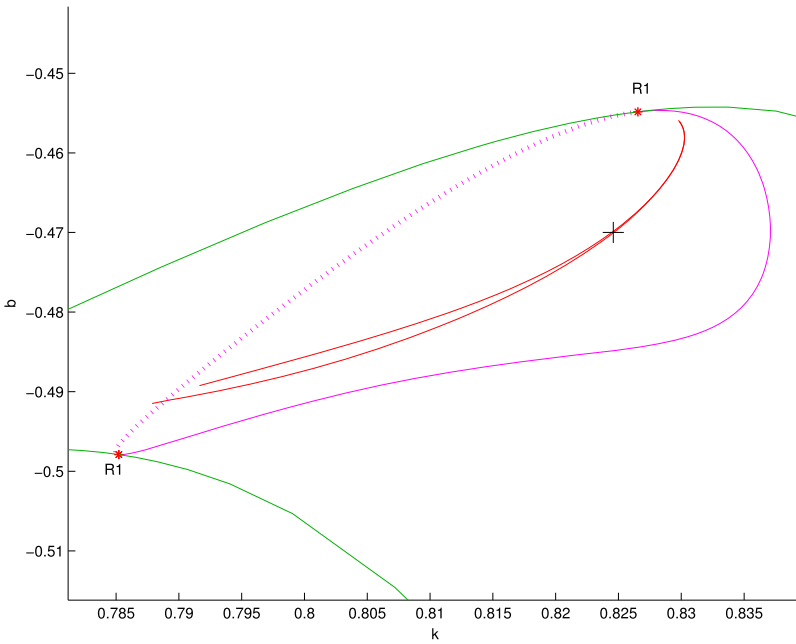
Fig. 13. Green, limit point curves; red, curves of homoclinic tangencies; magenta, Neimark-Sacker curve; dashed magenta, Neutral Saddle curve; black +, starting homoclinic tangency. The R1 points are 1:1 resonance points of the 5th iterate.
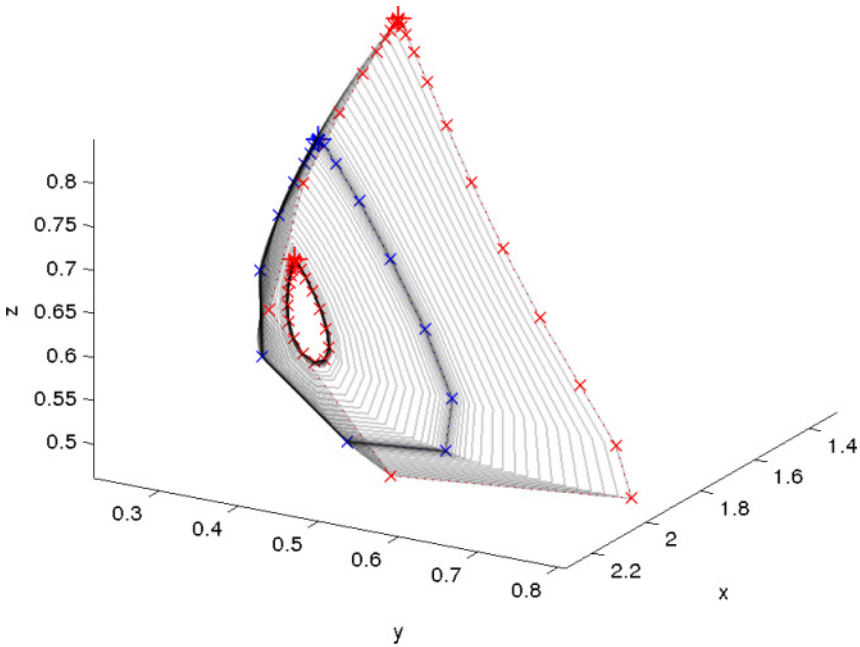

Fig. 14. Blue orbit, starting homoclinic tangency for $k = 0.82445996$, $b = -0.47$; smallest red orbit, homoclinic tangency close to R1 for $k = 0.82990325$, $b = -0.45615685$; largest red orbit, homoclinic tangency far away from R1 for $k = 0.79163754$, $b = -0.48923588$.
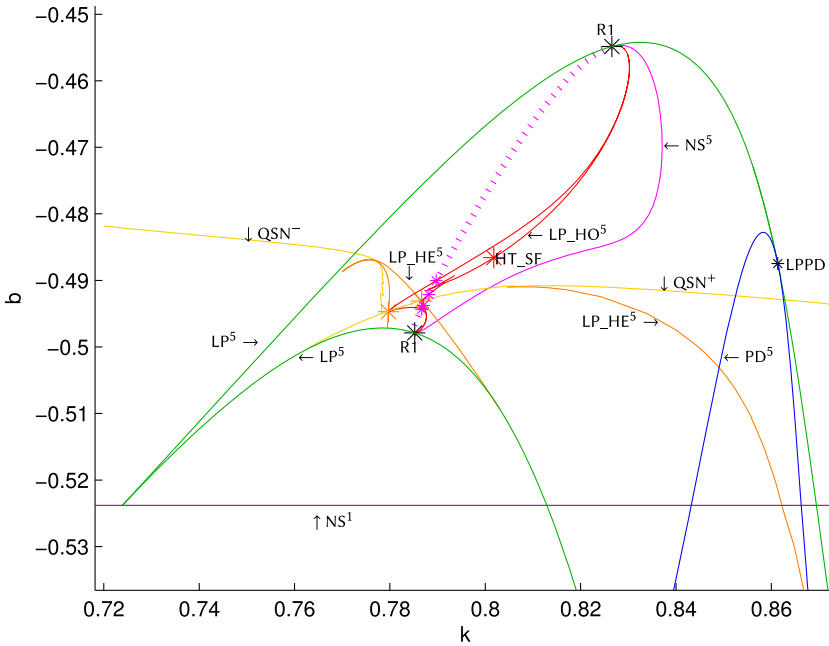
Fig. 15. The full resonance horn. The dark magenta curve (straight horizontal line) is a NS1 curve, all other curves are bifurcation curves of the 5th iterate. Green=LP5 curves; Magenta solid=NS5 curve; Magenta dashed=neutral saddle fixed points. The magenta curves touch the green curves in R1 points. Red=Homoclinic tangency curves LP_HO, rooted in the R1 points. Orange and yellow, heteroclinic tangencies. Blue=PD5. Note the presence of a HT_SF bifurcation point on the LP_HO curve, cf. Figure 6.

Figure 15 shows the full resonance horn and Figure 16 provides a zoom showing a remarkable interplay of local and global bifurcation curves. We have detected a HT_SF bifurcation point (big red star) at $(k, b) = (0.80179, -0.4866)$ and four HT_NS bifurcation points (small magenta stars) at $(k, b) = (0.789729826599800, -0.490045493902434)$, $(0.788197353086524, -0.492122114091179)$, $(0.787017631285026, -0.493787062295342)$, and $(0.786651451614289, -0.494323335473866)$, respectively. In addition, we have determined two other global bifurcation curves $QNS^{\pm}$ that indicate a quasi-periodic saddle-node bifurcation. Here a stable and unstable invariant curve coalesce and disappear. For this, we simulated the map starting close to the invariant curve. Then, we varied the parameters until the large attractor disappeared and the orbit ended up in the fixed point $(1, 1, 1 - b - k)$. For QNS^+ this yields a reasonably continuous boundary, although sometimes a resonance of a cycle with period above 50 was encountered. The boundary QNS^- has a much more complex structure, as we encountered many more resonances involving curves of heteroclinic tangencies for much higher periods. Notice that the curve LP_HE^5 extends toward the period-doubling bifurcation curve PD^5 where the period-5 saddle cycle has two unstable and one stable direction. Indeed, the geometry of the attractor seemed to be quite complicated in that area. We did not explore this situation in more detail.

Our results show for the first time the intricate details of an unfolding of a resonance bubble near a quasi-periodic saddle-node bifurcation. Several works have considered the unfolding of this resonance bubble from a theoretical perspective using approximating vector fields [2, 4–6]. In particular, these works predict a bifurcation structure for the cycles in the resonance tongue, as we find here too. In addition, there are bifurcations of invariant curves emerging from Neimark-Sacker
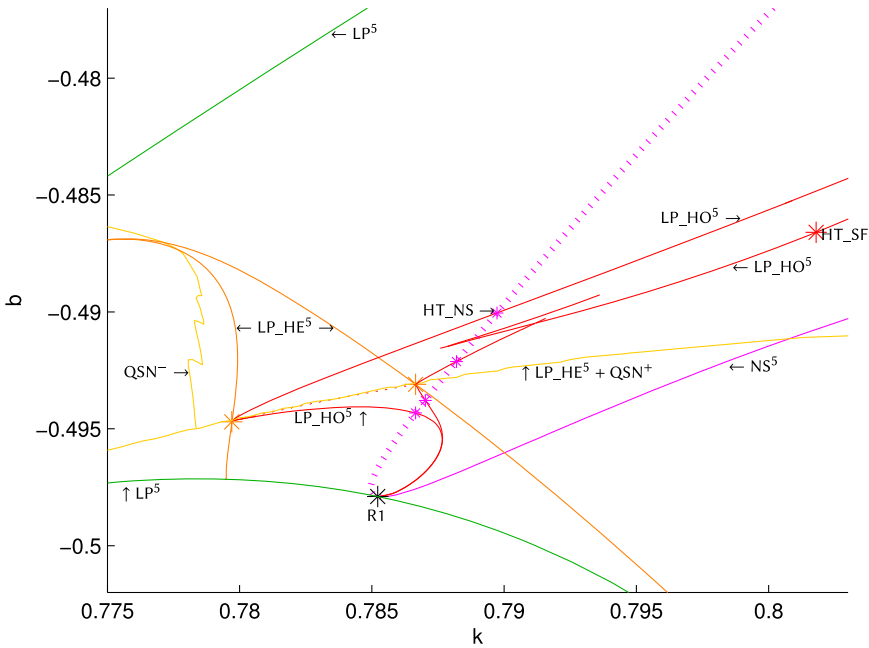
Fig. 16. Zoom of Figure 15. The four magenta crosses on the dashed magenta curve are HT_NS bifurcation points, cf. Figure 6. Note that the form of one of the LP_HO curves suggests the nearby presence of a swallowtail bifurcation of homoclinic orbits.

bifurcations and colliding onto homoclinic and heteroclinic connections. The theoretical unfolding shows a heteroclinic cycle, also called Necklace point. In the case of a vector field, the connecting orbit has codimension 1, i.e., forms a curve in a two-dimensional parameter space. For maps this curve is blown up to a homo-/heteroclinic zone with curves of homo-/heteroclinic tangencies as the boundary of this zone. Our results show that for maps one may expect two heteroclinic cycles consisting of such tangencies instead of the single heteroclinic cycle for a vector field. In addition, in the region where transversal connecting orbits coexist, we find chaotic dynamics. We should mention that we consider a cycle of period 5, whereas the theoretical predictions require period 7 or higher. Also the geometry of the manifolds seemed to suggest a more delicate structure. We will report on the details of resonance bubbles of cycles with higher periods elsewhere.

ACKNOWLEDGMENTS

REFERENCES

[1] B. Al-Hdaibat, W. Govaerts, and N. Neirynck. 2015. On periodic and chaotic behavior in a two-dimensional monopoly model. *Chaos Solitons Fractals* 70 (2015), 27–37. Retrieved from http://dx.doi.org/10.1016/j.chaos.2014.10.010.

[2] C. Baesens and R. S. MacKay. 2007. Resonances for weak coupling of the unfolding of a saddle-node periodic orbit with an oscillator. *Nonlinearity* 20, 5 (2007), 1283–1298. Retrieved from http://stacks.iop.org/0951-7715/20/i=5/a=012.

[3] W.-J. Beyn and J.-M. Kleinkauf. 1997. The numerical computation of homoclinic orbits for maps. *SIAM J. Numer. Anal.* 34, 3 (1997), 1207–1236. DOI : http://dx.doi.org/10.1137/S0036142995281693

[4] H. W. Broer, S. J. Holtman, G. Vegter, and R. Vitolo. 2011. Dynamics and geometry near resonant bifurcations. *Reg. Chaotic Dynam.* 16, 1 (2011), 39–50. DOI : http://dx.doi.org/10.1134/S1560354710520023

[5] A. Chenciner. 1987. Bifurcations de points fixes elliptiques—III. Orbites périodiques de n̓petites̓ périodes et élimination résonnante des couples de courbes invariantes. *Publications Mathématiques de l'IHES* 66 (1987), 5–91.

[6] A. Chenciner, A. Gasull, and J. Llibre. 1987. Une description complète du portrait de phase d'un modèle d'élimination résonante. *C. R. Acad. Sci. Paris Ser. I Math.* 305, 13 (1987), 623–626.

[7] A. Dhooge, W. Govaerts, and Yu. A. Kuznetsov. 2003. MATCONT: A matlab package for numerical bifurcation analysis of ODEs. *ACM Trans. Math. Softw.* 29, 2 (June 2003), 141–164. DOI : http://dx.doi.org/10.1145/779359.779362

[8] J. P. England, B. Krauskopf, and H. M. Osinga. 2004. Computing one-dimensional stable manifolds and stable sets of planar maps without the inverse. *SIAM J. Appl. Dynam. Syst.* 3, 2 (2004), 161–190. DOI : http://dx.doi.org/10.1137/030600131

[9] C. E. Frouzakis, R. A. Adomaitis, and I. G. Kevrekidis. 1991. Resonance phenomena in an adaptively-controlled system. *Int. J. Bifurcat. Chaos* 01, 01 (1991), 83–106. DOI : http://dx.doi.org/10.1142/S0218127491000075

[10] M. P. Golden and B. E. Ydstie. 1988. Bifurcation in model reference adaptive control systems. *Syst. Control Lett.* 11, 5 (1988), 413–430.

[11] S. V. Gonchenko, A. S. Gonchenko, I. I. Ovsyannikov, and D. V. Turaev. 2013. Examples of lorenz-like attractors in henon-like maps. *Math. Model. Natural Phenom.* 8, 05 (2013), 48–70.

[12] S. V. Gonchenko and V. S. Gonchenko. 2000. On andronov-hopf bifurcations of two-dimensional diffeomorphisms with homoclinic tangencies. *Preprint WIAS No. 556* (2000).

[13] S. V. Gonchenko, V. S. Gonchenko, and J. C. Tatjer. 2007. Bifurcations of three-dimensional diffeomorphisms with non-simple quadratic homoclinic tangencies and generalized Hénon maps. *Reg. Chaotic Dynam.* 12, 3 (2007), 233–266. DOI : http://dx.doi.org/10.1134/S156035470703001X

[14] V. Gonchenko, Yu. A. Kuznetsov, and H. G. E. Meijer. 2005. Generalized hénon map and bifurcations of homoclinic tangencies. *SIAM J. Appl. Dynam. Syst.* 4, 2 (2005), 407–436. DOI : http://dx.doi.org/10.1137/04060487X arXiv: http://epubs.siam.org/doi/pdf/10.1137/04060487X

[15] W. Govaerts, R. Khoshsiar Ghaziani, Yu. A. Kuznetsov, and H. G. E. Meijer. 2007. Numerical methods for two-parameter local bifurcation analysis of maps. *SIAM J. Sci. Comput.* 29, 6 (Oct. 2007), 2644–2667. DOI : http://dx.doi.org/10.1137/060653858

[16] W. Govaerts, Yu. A. Kuznetsov, H. G. E. Meijer, and N. Neirynck. 2011. A study of resonance tongues near a chenciner bifurcation using matcontm. In *Proceedings of the 7th European Nonlinear Dynamics Conference (ENOC'11)*, D. Bernardini, G. Rega, and F. Romeo (Eds.). Euromech.

[17] S. Hittmeyer, B. Krauskopf, and H. M. Osinga. 2013. Interacting global invariant sets in a planar map model of wild chaos. *SIAM J. Appl. Dynam. Syst.* 12, 3 (2013), 1280–1329.

[18] H. Kawakami. 1981. Algorithme numérique définissant la bifurcation d'un point homocline. *C. R. Acad. Sci. Paris* 293, 1 (1981), 401–403.

[19] R. Khoshsiar Ghaziani. 2008. *Bifurcations of Maps: Numerical Algorithms and Applications*. Ph.D. Dissertation. Ghent University. http://dx.doi.org/1854/9725.

[20] R. Khoshsiar Ghaziani, W. Govaerts, Yu. A. Kuznetsov, and H. G. E. Meijer. 2009. Numerical continuation of connecting orbits of maps in Matlab. *J. Dif. Equat. Appl.* 15, 8-9 (2009), 849–875.

[21] R. Khoshsiar Ghaziani, W. Govaerts, and C. Sonck. 2012. Resonance and bifurcation in a discrete-time predator-prey system with Holling functional response. *Nonlin. Anal. Real World Appl.* 13, 3 (2012), 1451–1465. http://dx.doi.org/10.1016/j.nonrwa.2011.11.009.

[22] B. Krauskopf and H. Osinga. 1998. Growing 1D and quasi-2D unstable manifolds of maps. *J. Comput. Phys.* 146, 1 (1998), 404–419. DOI : http://dx.doi.org/10.1006/jcph.1998.6059

[23] C. Mira. 1987. *Chaotic Dynamics*. World Scientific, Singapore.

[24] J. M. Ortega and W. C. Rheinboldt. 1970. *Iterative Solution of Nonlinear Equations in Several Variables*. Academic Press, New York. Reprint SIAM 2000.

[25] J. K. Wróbel and R. H. Goodman. 2013. High-order adaptive method for computing two-dimensional invariant manifolds of three-dimensional maps. *Commun. Nonlin. Sci. Numer. Simul.* 18, 7 (2013), 1734–1745.

[26] K. Yagasaki. 1998. Numerical detection and continuation of homoclinic points and their bifurcations for maps and periodically forced systems. *Int. J. Bifurcat. Chaos* 08, 07 (1998), 1617–1627. DOI : http://dx.doi.org/10.1142/S0218127498001285 arXiv: http://www.worldscientific.com/doi/pdf/10.1142/S0218127498001285

[27] T. Yoshinaga, H. Kitajima, H. Kawakami, and C. Mira. 1997. A method to calculate homoclinic points of a two-dimensional noninvertible map. *IEICE Trans. Fund. Electron. Commun. Comput. Sci.* 80, 9 (1997), 1560–1566.